

Aggregation and fragmentation dynamics in random flows: From tracers to inertial aggregates.

Ksenia Guseva^{1,*} and Ulrike Feudel^{1,†}

¹*Theoretical Physics/Complex Systems, ICBM, University of Oldenburg, 26129 Oldenburg, Germany*

We investigate aggregation and fragmentation dynamics of tracers and inertial aggregates in random flows leading to steady state size distributions. Our objective is to elucidate the impact of changes in aggregation rates, due to differences in advection dynamics, especially with respect to the influence of inertial effects. This aggregation process is, at the same time, balanced by fragmentation triggered by local hydrodynamic stress. Our study employs an individual-particle-based model, tracking position, velocity and size of each aggregate. We compare the steady-state size distribution formed by tracers and inertial aggregates, characterized by different sizes and densities. On the one hand, we show that the size distributions change their shape with changes of the dilution rate of the suspension. On the other hand, we obtain that the size distributions formed with different binding strengths between monomers can be rescaled to a single form with the use of a characteristic size for both dense inertial particles and tracer monomers. Nevertheless, this last scaling relation also fails if the size distribution contains aggregates that behave as tracer-like and as inertial-like, which results in a crossover between different scalings.

I. INTRODUCTION

Aggregation and fragmentation dynamics in turbulent flows is found at the core of many processes in environmental and engineering sciences. Examples of such systems include the formation of rain droplets in clouds [1], the settling of marine aggregates in estuaries and open ocean [2, 3], and even growth of stars and galaxy formation by dust particle collisions [4]. In all these cases, the balance between aggregation and fragmentation dynamics determines the characteristics of the population of particles — such as aggregate size distribution — in the steady-state. While different mechanisms can be identified to be responsible for breakups (e.g. instability after reaching a certain size, or due to the action of hydrodynamic forces), aggregation always results from collisions, and hence depends on the advection of aggregates by the velocity field.

In this work we analyze the steady-state size distribution produced by the competition between aggregation and breakup by hydrodynamic stress for aggregates subjected to different advection dynamics (tracers in contrast to inertial aggregates). We use an *individual-particle-based* model where each aggregate is moved independently in space, and at each instant in time is identified with a position, a velocity and a size. This approach was previously used to investigate the influence of different fragmentation mechanisms on aggregation-fragmentation dynamics of small inertial aggregates in random [5, 6] and convection flows [7, 8]. Here we choose a single mechanism for fragmentation — breakup due to hydrodynamic stress, and focus on the influence of changes in aggregation rates on the steady-state size distribution. With this aim, we consider particles that move

differently while advected by the flow field and therefore have distinct collision (aggregation) rates. These types of particles can be classified into tracers and inertial aggregates. Tracers are particles that follow the velocity field exactly, identically to fluid elements. Inertial aggregates, on the contrary, deviate from the fluid trajectories due to action of several hydrodynamic forces. One important characteristic unique to inertial aggregates is that their motion depends strongly on their size.

Several recent studies have theoretically evaluated the aggregation rates for both tracers [9] and for inertial particles [10] in the absence of fragmentation dynamics. For inertial particles in particular, the collision dynamics is known to be strongly enhanced in turbulence due to phenomena such as *preferential concentration* [11, 12] and *caustics* [1, 13, 14], for a review see [15]. Other studies have estimated fragmentation rates, when these are triggered by hydrodynamic forces in the absence of aggregation, although only for tracer particles [16, 17]. Aggregation and fragmentation processes are brought together only within a mean field approximation using *population balance equations*, which are able to determine the size distribution as a function of time for a reversible aggregation process [16, 18–20]. Although significant progress can be achieved with this approach, it cannot account for spatial fluctuations in particle numbers, which are enhanced by inertial effects and for the location-dependent fragmentation rates. Therefore we propose to treat the aggregation and fragmentation as coupled processes, taking fully into account the spatial variations in distribution and sizes of aggregates by means of an *individual-particle-based* model.

Our aim is to investigate the consequences of inertia on the steady-state of aggregation and fragmentation processes. We are interested in the case where breakup of aggregates occurs due to hydrodynamic forces, using a random flow field mimicking turbulence. We use different ensembles of inertial monomers (primary, unbreakable particles), and explore the influence of Stokes num-

* ksenia.guseva@uni-oldenburg.de

† ulrike.feudel@uni-oldenburg.de

ber and density on the steady state, which result from differences in advection dynamics. We show the changes induced in the dynamics and their results in the scaling of the mean size and other characteristics of the size distribution. We analyze the scaling properties of the size distribution with respect to the resistance of aggregates to hydrodynamic forces and to the dilution of the suspension for ensembles of aggregates with different inertial properties.

This paper is organized as follows. Sec. II consists of implementation details of the *individual-particle-based* model. It is divided in Subsect. II A, where we describe the advection of inertial particles, and Subsects. II B and II C, where we describe the details for the aggregation and fragmentation processes. We proceed with the results for the influence of the dilution rate of the suspension for the aggregation-fragmentation dynamics of tracer and of inertial aggregates in Sec. III A. Finally we analyze the effect of the binding strength between monomers in Subsect. III B 1 and Subsect. III B 2, again comparing the steady state properties of ensembles of aggregates with different advection dynamics. The comparison and a summary of the impact of advection dynamics and results for other ensemble types are presented in Subsect. III B 3. We conclude and then discuss the results in Sec. IV.

II. METHODS AND THEORETICAL INTRODUCTION

We start by presenting details of the three dynamical processes which compose our model: advection, aggregation and fragmentation. Our system consists of particles which are advected by the flow while aggregating with each other upon collisions, and fragmenting due to local forces in the flow field. This section is divided into three parts: first we describe the advection dynamics in Subsect. II A; then we proceed in Subsect. II B with the general aspects of the aggregation and fragmentation dynamics; finally in Subsect. II C we provide details of the forces that drive fragmentation events.

A. Advection of inertial particles

We assume that all aggregates are immersed in a moving fluid and advected by it. As the flow field, $\mathbf{u}(\mathbf{X}, t)$, we use a random (synthetic) flow [21–23] which mimics homogeneous isotropic turbulence in the dissipative scale. It corresponds to a Gaussian incompressible velocity field generated by means of random perturbations of Fourier modes. Details of the implementation of this random flow field can be found in Appendix I. The important parameters which characterize the flow are: τ_f – correlation time; λ_f – correlation length; and u_0 – mean of the absolute velocity. These three parameters can be combined into a single dimensionless parameter: the Kubo num-

ber, $Ku = u_0\tau_f/\lambda_f$, which characterizes the persistence of coherent structures in the flow field with respect to the time needed for fluid particles to explore them [15].

We assume a dilute suspension of small spherical particles, which are much smaller than the smallest coherent structures (eddies) of the flow. On the one hand we consider particles which follow the flow field exactly. Their trajectories can be obtained from: $\dot{\mathbf{X}} = \mathbf{u}(\mathbf{X}, t)$. These particles are called *tracers*. On the other hand, we look at particles whose trajectories may deviate from flow field trajectories due to inertial effects. The motion of these inertial particles can be described by the following equations

$$\dot{\mathbf{X}} = \mathbf{V} \quad \dot{\mathbf{V}} = \beta D_t \mathbf{u}(\mathbf{X}, t) - \frac{1}{\tau_p} (\mathbf{v} - \mathbf{u}(\mathbf{X}, t)), \quad (1)$$

where \mathbf{X} , \mathbf{V} correspond to the position and the velocity of a particle respectively. Eq.(1) are an approximate form of the Maxey-Riley equations and are valid in the limit of small particle Reynolds numbers. They were formulated independently by Gatinol [24], Maxey & Riley [25] and later corrected by Auton [26]. The abbreviation $D_t = \partial_t + \mathbf{u} \cdot \nabla$ represents the derivative along the flow trajectory. The ratio between aggregate's ρ_0 and fluid's ρ_f densities is given by the parameter $\beta = \frac{3\rho_f}{\rho_f + 2\rho_0}$. The time it takes for an aggregate to adjust to the changes of the flow is given by the Stokes time τ_p , which depends on the aggregate's size r_p . This response time can be compared to the smallest time scale of the flow τ_f . The relation between these two time scales gives a dimensionless number, the Stokes number:

$$St = \frac{\tau_p}{\tau_f} = \frac{r_p^2}{3\beta\nu} \frac{1}{\tau_f}, \quad (2)$$

with ν as the kinematic viscosity. While tracers are distributed homogeneously in space, inertial particles segregate into random attractors due to dissipation (Fig. 1). For a review of the dynamics of inertial particles in random flows, and the mechanisms which drive the segregation such as *preferential concentration* [11, 12, 27, 28] and random amplification [29] see [15].

The segregation into fractal attracting regions is a well established explanation for the fast growth of rain droplets in clouds, since it would strongly increase the number of collisions and consequently the aggregation rates [1, 30]. This increase has already been demonstrated for inertial particles in random flows [10]. Our objective is to explore the consequence of an increased aggregation rate on size distributions which results from aggregation and fragmentation dynamics.

B. Aggregation-fragmentation dynamics

The dynamics of each aggregate is modeled *individually*, and we attribute to each one of them, at each instant

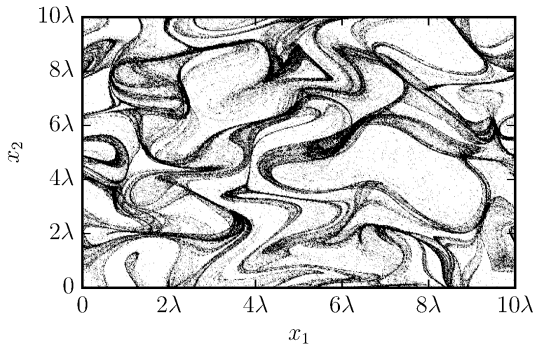


FIG. 1. Non-homogeneous spatial distribution of inertial particles, with $St = 0.5$ for a flow field with $Ku = 1$.

of time, — a position, a velocity and a size. For convenience the sizes of all aggregates in the system are measured with respect to a unit particle — the monomer. We assume that all monomers are small spheres with a radius r_0 and mass m_0 ($m_0 = \frac{3\rho_0}{4\pi r_0^3}$, where ρ_0 is the monomer's density). Their main property is that they cannot be broken. However they can form large aggregates since they can stick together upon collision and hence, build an ensemble of aggregates with different sizes in the suspension. Therefore, each aggregate in the system can be described by an *integer* number α of monomers that compose it. In other words, α establishes a relation between the size of an aggregate and the unit size, hence specifying the aggregate's mass as $m_\alpha = \alpha m_0$, and its radius as $r_\alpha = \alpha^{1/3} r_0$. Here we assume that each aggregate is a sphere. According to this each of the aggregates has its specific Stokes number $St_\alpha = \frac{r_\alpha^2}{3\beta\nu} \frac{1}{\tau_f}$,

While two aggregates, of radius r_i and r_j (with i and j monomers respectively) move, they may approach each other. When the relative distance d between them becomes equal to $r_i + r_j$ a collision occurs. We assume that each of such collision events, results in aggregation, where a new particle of size $\alpha = i + j$ is formed. We postulate that in all aggregation events the mass and the momentum are conserved, and from this condition we can derive all the properties of the resulting aggregate. Furthermore, all aggregates have a spherical shape independently of their size and the same density, ρ_0 , as the monomers which form them. To be able to track all the collisions efficiently we use an event-driven algorithm, a detailed description of it can be found in [21].

Fragmentation, alternatively, is driven by an external force exerted on the aggregate, which depends on the position of the aggregate in space; the details about this force are presented in Subsec. II C. In these breakup events two smaller aggregates of similar size are produced (binary fragmentation), so that mass conservation is obeyed. These fragments are placed withing a close distance of each other. Their velocity is kept the same as of the aggregate before break-up to ensure momentum conservation. Fragmentation and aggregation are com-

peting processes, and the balance between them leads to a steady state size distribution of aggregates in the suspension, containing N_α aggregates with a particular size α .

We initialize our suspensions always with homogeneously spread monomers, $N_1(0) = M$ and $N_\alpha = 0$ with $\alpha \neq 1$, where M is the total number of monomers. Then we track the time evolution of the number of aggregates in each size class $N_\alpha(t)$ resulting from advection of monomers and aggregation, see Fig. 2 (a). The transient dynamics consists of an initial period of irreversible aggregation, followed by an increase in fragmentation events. These breakage events become more and more relevant as the sizes of aggregates in the suspension increase. The number of fragmentation events grows until, on average, it balances all aggregation events and the dynamics reaches a steady state. The time to reach this balance depends again on the number and properties of monomers initialized in the suspension. The resulting steady state size distribution is characterized by an average aggregate size $\langle \alpha \rangle_e$ and a size distribution of aggregates, Fig. 2 (b). To eliminate time fluctuations of $\langle \alpha \rangle_e$, we define a time average computed for the interval T (after discarding transients), i.e. $\langle \cdot \rangle_t = \int_t^{t+T} \langle \cdot \rangle_e(t') dt'$. In Fig. 2 (a, b) we show an example of the evolution of the size distribution in time and the corresponding steady state size distribution respectively.

It is interesting to note that the traditional mean field approach for aggregation-fragmentation dynamics using certain kernels predicts that the size distribution in the steady state obeys a scaling relation with respect to a characteristic particle size [31–34]. In our case the prediction is

$$N_\alpha = \frac{1}{\alpha^2} f(\alpha / \langle \alpha \rangle_e). \quad (3)$$

Additional scaling properties can also be derived for $\langle \alpha \rangle_e$, establishing that it scales as a power law with the total number of monomers in the suspension M . Moreover, it scales as a power law with the strength of the binding forces inside the aggregate. Our objective is to verify if this scaling form of the size distribution holds also for our individual particle approach, which takes the spatial distribution of aggregates explicitly into account. By contrast, the mean field approach is based on aggregation rates which are independent of the spatial distribution of aggregates.

C. Fragmentation by hydrodynamic stress

We are interested in a specific type of fragmentation process in which breakup events develop from interactions of aggregates with the local flow field. In our study the flow is responsible for two types of dynamics: (i) it carries particles around so that they can meet and aggregate and; (ii) it exerts forces that act on the particle's structure, being able to trigger breakups. For

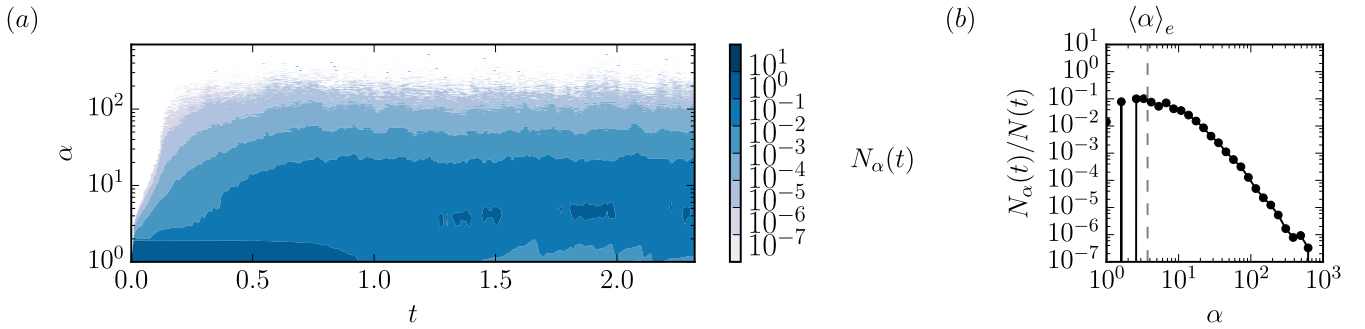


FIG. 2. (a) Evolution of the size distribution in time. (b) size distribution of aggregates in the steady state, the dashed gray line represents the mean aggregate size $\langle \alpha \rangle_e$. N is the total number of aggregates in the system ($N = \sum_{\alpha} N_{\alpha}$).

such type of fragmentation, numerous studies point to a strong link between fragmentation rates of aggregates and their morphological properties, such as shape, porosity and more importantly their size, see [35, 36]. The hydrodynamic stress that drives the breakup events is the shear force, defined as $S = (2 \sum_i \sum_j S_{ij} S_{ij})^{\frac{1}{2}}$, where $S_{ij} = \frac{1}{2} \left(\frac{\partial u_i}{\partial x_j} + \frac{\partial u_j}{\partial x_i} \right)$ corresponds to the rate-of-strain tensor of the flow field, $\mathbf{u}(\mathbf{X}, t)$ [37]. The shear force varies in space and time, and has predefined statistical properties, such as a probability distribution [38]. For the random flow used in this study, this probability distribution of the shear forces is shown in Fig. 3 (a).

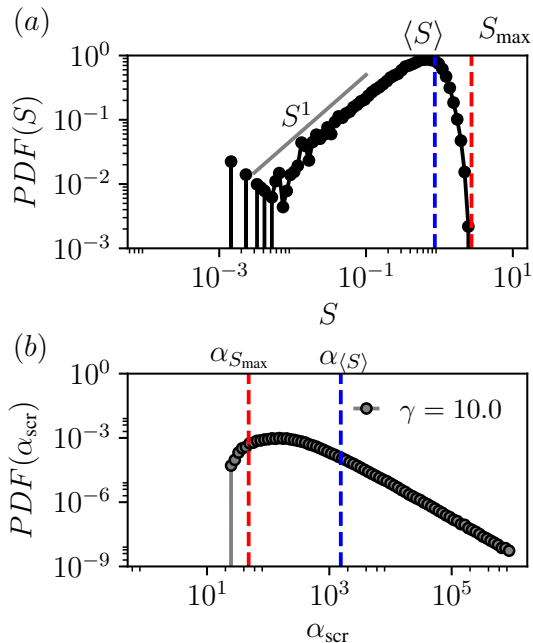


FIG. 3. (a) PDF of the shear forces for a random flow, obtained from space sampling of $\mathbf{u}(\mathbf{X}, t)$, with $Ku = 1$ ($\tau_f = 1$) and (b) the corresponding maximum aggregate's size allowed by these forces, the parameters used are $\gamma = 10$ and $\kappa = 3$.

As described previously we prescribe the existence of

a smallest aggregate's size, the monomer, which cannot be broken by the shear forces of the flow field. All other, larger aggregates in the suspension produced by means of aggregation of these monomers are subject of fragmentation. The monomers inside an aggregate are hold together by internal binding forces. When the shear forces of the flow field, which act on the aggregate, are stronger than these binding forces a fragmentation event occurs. Therefore we can define a critical shear S_{cr} at which the shear force becomes larger than the binding forces resulting in fragmentation. Importantly, this S_{cr} depends on the size of the aggregate. Moreover, the functional form of the critical shear relies on the assumption that large aggregates are more likely to break than the smaller ones and therefore are more sensitive to fluctuations of the shear in the flow.

We use a power law relation between the critical shear and the aggregate size,

$$S'_{cr} = \gamma' \alpha^{-\frac{1}{\kappa}}, \quad (4)$$

where α is the number of monomers in the aggregate, and the additional parameter γ' and the exponent κ represent the dependence on other morphological properties. This relation, taken from literature [39, 40], results from numerical simulations of individual aggregates as well as experiments, by taking into account the complex fractal structure of aggregates and its internal binding forces, in different flow fields. We assume that all aggregates fragment into two smaller ones with similar sizes (binary fragmentation). The time scale on which a breakup occurs is supposed to be significantly shorter than all other relevant time scales of the dynamics. Therefore we approximate each breakup event as instantaneous, and assume that it occurs exactly at the point where the aggregate experiences a shear stress that exceeds the critical value. Furthermore, if the shear stress is still larger than the binding forces of any of produced fragments, another fragmentation event is performed within the same time step. This can result in a fragmentation cascade, which proceeds until all produced fragments are able to resist to local shear. For convenience we work with a relative critical shear value, by comparing it with the mean shear rate

of the flow $\langle S \rangle$. We assign $S_{cr} = S'_{cr} / \langle S \rangle = \gamma \alpha^{-\frac{1}{\kappa}}$, with $\gamma = \gamma' / \langle S \rangle$. Note that, with the use of this rescaling, $\gamma \leq 1$ corresponds to the case where for any α , $S'_{cr} < \langle S \rangle$. We have fixed the value of the exponent $\kappa = 3$ in our simulations, which corresponds to solid spheres, according to [41].

To facilitate our analysis we highlight here some of the relations between the shear distribution of the random flow and the sizes of aggregates produced. The PDF of shear, obtained from space sampling of $\mathbf{u}(\mathbf{X}, t)$, is shown in Fig. 3 (a). For shear values below average it can be described as a linearly increasing function: $\text{PDF}(S < \langle S \rangle) \propto S^\chi$, with $\chi = 1$. Otherwise for $S > \langle S \rangle$ the probability distribution decreases sharply and has a cutoff at $S_{\max} \sim 3 \langle S \rangle$, which is an approximation of the asymptotic cutoff seen in Fig. 3 (a). This aspect differs significantly from the behaviour of a homogeneous and isotropic turbulent flow, where the shear distribution assumes a broader shape, and has an exponential decay for $S > \langle S \rangle$ [42], reaching values as large as hundred times of the average shear. This can be noticed from the appearance of extreme and rare events where the shear value suddenly rises. Such events are specific to turbulence and are absent in random flows. For more details about this comparison and how it reflects on fragmentation rates of tracer particles, see [17].

With a fixed κ ($\kappa = 3$), we can attribute to each γ corresponding size classes which facilitate the connection of the aggregate's size distribution to the properties of the flow: $\alpha_{\langle S \rangle}$ – featured as a dashed blue line on the size distribution in Fig. 3 (b), corresponds to the size class with $S_{cr} = \langle S \rangle$; and $\alpha_{S_{\max}}$ – represented as a dashed red line in Fig. 3 (b), shows the size class with $S_{cr} = S_{\max}$. It is also important to note that the smallest size in the suspension in steady state is $\sim \alpha_{S_{\max}}/2$ since we work with binary fragmentation where the resultant fragments are nearly of the same size, except for small fluctuations.

Let us discuss the limiting case of the broadest size distribution of aggregates. Since this size distribution depends only on the properties of the flow, we take a snapshot of the flow field at one arbitrary time instant. For this snapshot we determine the spatial distribution of the shear forces in the flow. Suppose we distribute to each location in space one aggregate whose size is the largest possible i.e. its size α is determined by the critical shear at its position. As an example, let the considered position be (x_0, y_0) and the shear at this position be $S(x_0, y_0) = \left(2 \sum_i \sum_j S_{ij}(x_0, y_0) S_{ij}(x_0, y_0)\right)^{1/2}$, then the corresponding size α at this position would be $\alpha(x_0, y_0) = \left(\frac{1}{\gamma} S(x_0, y_0)\right)^{-3}$. Taking now aggregates on all positions (x, y) in configuration space fulfilling the condition of the maximum possible size before breakup we obtain the broadest possible size distribution. In case of our random flow for $\alpha > \alpha_{\langle S \rangle}$ this strong aggregation limit, taking into account that $\text{PDF}(S < \langle S \rangle) \propto S^\chi$, produces a size distribution $N_\alpha \propto \alpha^{-(\chi + \kappa + 1)/\kappa}$. Which for $\kappa = 3$ and $\chi = 1$, has the form $N_\alpha \propto \alpha^{-5/3}$ (see Fig. 3 (b)

and red stars in Fig. 6 (a)). This power law is the broadest size distribution allowed by the shear of the flow. In the next section we show that decreasing the dilution rate or increasing particle's inertia and particle's segregation brings the size distribution closer to this limit.

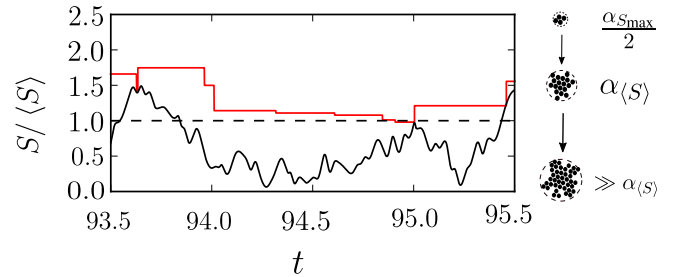


FIG. 4. Schematic representation of the changes in critical shear attributed to an aggregate, which changes due to aggregation and fragmentation events (red), in comparison to the shear force of the flow at the aggregate's position (black).

Finally, we would like to emphasize that the lifetime of an aggregate does not only depend on its size, but also correlates with the time scales of the flow field. For this purpose it is useful to follow an individual aggregate (in what is also known as the Lagrangian view). We can monitor the shear forces this aggregate experiences while advected by the flow field, and additionally, how this aggregate changes its size during this time due to aggregation and fragmentation events. Those events lead to transitions between size classes, see Fig. 4. This view allows us to compare the time scales between aggregation-fragmentation events and the time scale of the flow. In fact, for a random flow the Lagrangian velocity becomes uncorrelated after a time span proportional to the correlation time τ_f or an eddy turnover time λ_f/u_0 . Therefore the sampling of the possible shear values depends only on these two time scales in this simple set-up. For instance a tracer starting at a region of the flow with low shear will, after a time interval proportional to τ_f , move into a region with high shear value. As a consequence, the time an aggregate has to grow is finite, and restricted by the flow time scales. Here we argue that the number of aggregation events happening while the aggregate is entering a region of small shear is crucial to describe the tail of the aggregate size distribution. Furthermore, the lifetimes of large aggregates get smaller than τ_f , beyond $\alpha_{\langle S \rangle}$. In other words such large particles are fragmented by the flow in a time span smaller than the correlation time of the flow, Fig. 4.

III. RESULTS

A. Dilution rate

In this Subsection we compare the steady state size distributions obtained for tracers and inertial monomers.

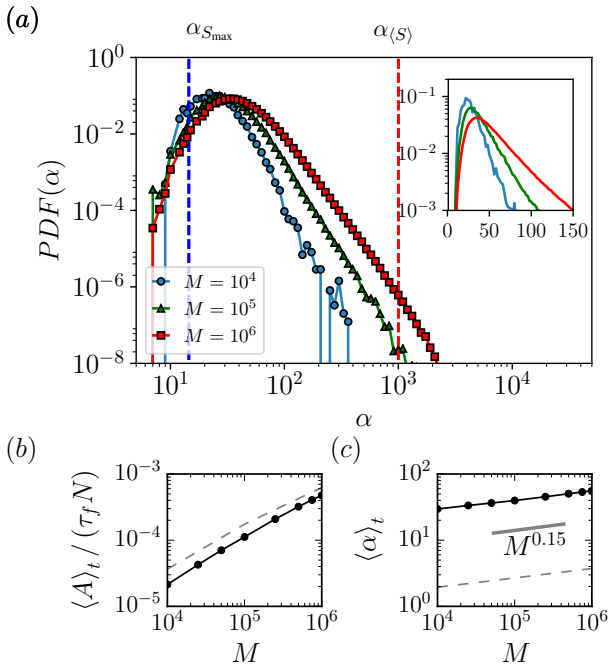


FIG. 5. (a) Steady state size distribution of non inertial (tracer) aggregates obtained by changing the number of monomers in the flow, in the inset the same in log-lin representation; (b) Number of aggregation (or fragmentation) events per aggregate in one correlation time of the flow; (c) Average aggregate size as a function of the total number of monomers in the suspension. Tracer monomers characterized by a size $r_0 = 5 \cdot 10^{-4} \lambda_f$ and binding strength $\gamma = 10$ (solid lines) and $\gamma = 4$ (gray dashed lines in (b) and (c)).

We analyze the influence of the total number of monomers M on the aggregation and fragmentation processes, and the resulting size distribution in the steady state.

We start by showing the resulting steady state size distributions for tracer monomers, Fig. 5 (a). It is important to highlight two main characteristics which distinguish the dynamics of tracers from inertial aggregates: (1) the size of a tracer aggregate does not influence the advection of this aggregate by the flow; (2) tracer aggregates are distributed uniformly in space when advected by an incompressible flow field. Taking into account these aspects, the appearance of spatial inhomogeneities in the concentration of aggregates, for the tracer system can only result from aggregation and fragmentation dynamics. In view of decreasing the simulation time, a large part of these simulations for tracer monomers were run with $\gamma = 10$. As explained previously (see Sec. II C) the size distribution is characterized by a minimum size $\sim \alpha_{S_{\max}/2}$, where S_{\max} is a function of γ . As we increase the number of monomers in the suspension, $\langle \alpha \rangle_t$ increases and the size distribution gets broader. We identify that the average size scales as $\langle \alpha \rangle_t \propto M^{0.15}$, Fig. 5(c). The differences are not only observed in the averages,

but also in the dynamics of the steady state, which also changes with the number of monomers in the suspension: we observe that the number of aggregation (fragmentation) events increases with M . We have counted the total number of aggregation events in the system in a correlation time A , and obtained an average for the number of these events per aggregate in one correlation time in the steady state $\langle A/N \rangle_t$, where $N = \sum_{\alpha} N_{\alpha}$. In Fig. 5(b), we show how the average number of events per aggregate changes with the increase of total number of monomers in the system. Note that for the steady state the number of fragmentation events per aggregate is on average the same as of aggregation events.

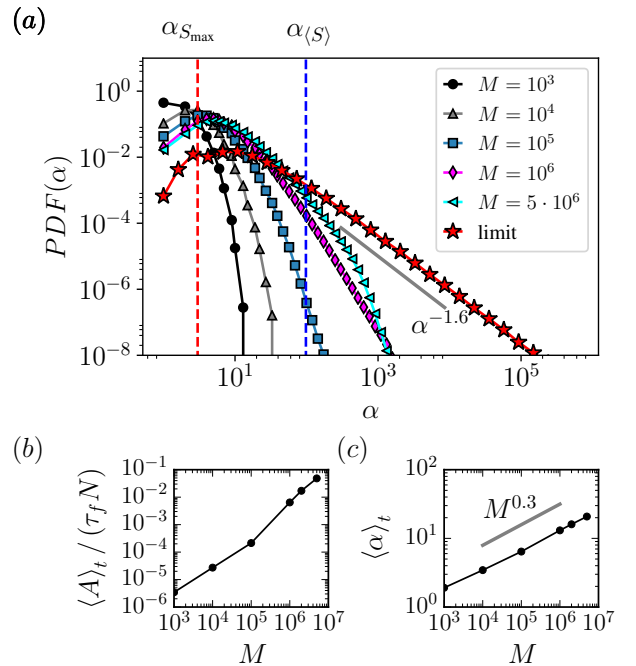


FIG. 6. (a) Size distributions of aggregates initialized with different numbers of monomers M , for monomers with $r_p = 5 \cdot 10^{-4} \lambda_f$, $\beta = 0.1$, which corresponds to $St = 0.8$ and binding strength $\gamma = 4$. The size distribution represented with red stars corresponds to the limit distribution, described in Sec. II C. (b) Number of aggregation (or fragmentation) events per aggregate in one correlation time of the flow; (c) Average aggregate size as a function of the total number of monomers in the suspension.

For a system with inertial monomers not only aggregation and fragmentation dynamics depend on the position of these aggregates, but the advection dynamics depends on the aggregate's size too. Furthermore, the spatial fluctuations in aggregate numbers may be additionally enhanced by inertial effects, such as preferential concentration, which in turn affects the collision rates. As in previous paragraph we address the question of how the total number of monomers influences the size distributions of aggregates.

The steady state that results from interactions of in-

ertial aggregates in strongly diluted suspensions with $M = 10^3$ monomers, is characterized by a size distribution with a tail that appears to exhibit an exponential decay (Fig. 6 (a)). The steady state here is characterized by a small number of aggregation events A per aggregate in a correlation time of the flow, see Fig. 6 (b). As we increase the total number of monomers the effects of inertia get more noticeable. These effects are reflected in the average size of aggregates in the suspension, which for inertial aggregates increases as $M^{0.3}$, see Fig. 6 (c). The observed broad size distributions are a result of: an enhancement of collisions due to distinct reactions times that the aggregates of different sizes have to the flow field and also due to preferential concentration, which is effective only for some of the size classes. As we have discussed in Sec. IIC the fragmentation dynamics is coupled to the flow field, which has a preassigned correlation time τ_f . To grow up to sizes larger than $\alpha_{(S)}$, aggregates have to experience several aggregation events within τ_f . Therefore a simple consequence of large numbers of monomers (such as for $M = 10^6$, see Fig. 6 (a)) is a broad distribution tail, with sizes that can reach values larger than $\alpha_{(S)}$. However, from changes in the shape of the size distribution we can notice that the relation between aggregation and fragmentation dynamics is non trivial. Although, the number of both type of events are the same on average, the sizes involved in aggregation and fragmentation dynamics change. We can observe that large aggregates need longer times to form, since they result from sequences of aggregation events. However, they are characterized by very short “lifetimes” (much shorter than τ_f). As a consequence, even if large aggregates are formed in a correlation time they are quickly fragmented after their formation. In spite their short appearance in the suspension, their formation transforms the size distribution’s tail into a power-law-like shape.

As a result, for the case of tracers and especially of inertial aggregates, the shape of the size distribution depends strongly on the dilution rate of the suspension.

B. Influence of the binding strength

1. Tracer monomers

As stated previously the main parameter that linearly changes the resistance of all aggregates to shear forces in the flow, is the binding strength among monomers, represented by parameter γ . While an increase in γ also means that aggregates are more resistant to fragmentation, the result is a size distribution with a larger mean number of aggregates, $\langle \alpha \rangle_t$, in the steady state of the process. Furthermore, as γ increases we create aggregates with $\alpha > 1$, which are resistant even to the strongest hydrodynamic forces exerted by the flow field. These aggregates end up functioning as the smallest units in the ensemble, and can therefore be considered as “effective monomers”. For an ensemble of tracers these “effective monomers” will have

all properties identical to the original monomers, with the exception to their radius, $r_\alpha > r_p$. The outcome is a similar system, but with a smaller number of “effective monomers” and a different relation between “effective monomer” size r_α and the size of the vortices λ_f .

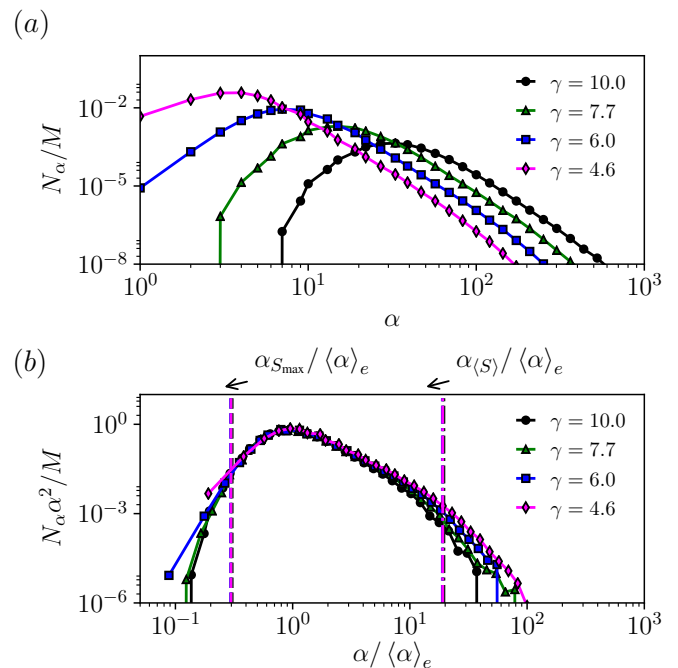


FIG. 7. Steady state size distributions of tracer aggregates for different binding strengths γ . Tracer monomers are characterized by a size $r_p = 5 \cdot 10^{-4} \lambda_f$ in a suspension with $M = 10^6$. (a) The size distribution in its original form. (b) Rescaled size distribution according to Eq.(3).

For tracers we chose to work with $M = 10^6$, since their dynamics is characterized by long transients. The large duration of transients is a consequence of small collision rates, due to the homogeneous spread of aggregates in space. Here we use the relation given by Eq.(3), to rescale the obtained size distributions. The size distribution in this form possesses a horizontal axis which is divided by $\langle \alpha \rangle_e$, a quantity that also grows with γ . The scaling of $\langle \alpha \rangle_e$ with the binding strength is discussed in more detail in Subsec. III B3. The tendency for all our study cases, therefore, is to have broader distributions for larger γ values (Fig. 7 (a)). In particular for tracers the average and the standard deviation (first and second moments of the size distribution) grow with the same proportion. We obtain a partial overlap of distributions in their rescaled form for different values of γ , Fig. 7 (b), with deviations only in the tail of the distribution. In this case, the size distribution has a sharper decrease towards larger aggregates and fewer aggregates that grow beyond $\alpha_{(S)}$. The maximum value is only four times larger than $\alpha_{S_{\max}}$ and we observe a narrow distribution. Note that for all dilution rates used, $\langle \alpha \rangle_e$ is only slightly above $\sim \alpha_{S_{\max}}/2$. Furthermore, the largest fraction of the

system's monomers remains in aggregates of sizes below $\sim \alpha_{(S)}$, characterizing a regime of few aggregation events per τ_f . The steady state size distribution can be rescaled with respect to the characteristic size of aggregates in the steady state, which in this case can be either the average aggregate $\langle \alpha \rangle_e$ or the “effective monomer”.

2. Inertial monomers

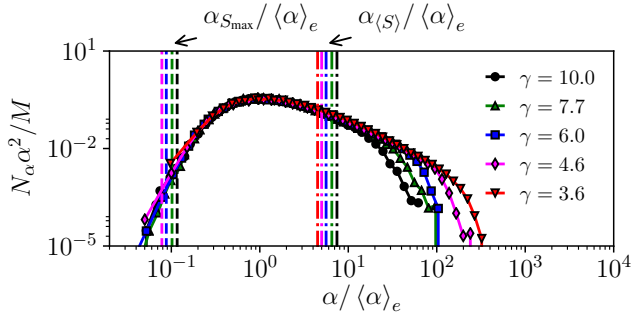


FIG. 8. Steady state size distributions N_α changing γ , binding strength among monomers. The data is scaled using the average aggregate size in the distribution $\langle \alpha \rangle_e$, according to Eq.(3). The simulations contains inertial aggregates ($St = 0.83$, $\beta = 0.1$) in suspension with $M = 10^6$ monomers.

Next we compare the steady state distribution for ensembles of inertial monomers characterized by different binding strengths. We initialize a suspension with $M = 10^6$ monomers. We again check the rescaled form of the size distribution, according to Eq.(3), using $\langle \alpha \rangle_e$ as the characteristic size. As for the case of tracers the use of this scaling collapses all size distributions with deviations appearing only in the tail, see Fig. 8.

The aggregation and fragmentation dynamics produces a mass flux flowing towards sizes much larger than $\alpha_{(S)}$. As we described in Sec. II C, for this set-up an aggregate may have sufficient time to grow before the flow decorrelates and exposes it to a high shear rate. Here one correlation time of the flow is enough for aggregates to grow into sizes much larger than $\alpha_{(S)}$. We observe that the flux of mass towards sizes larger than $\alpha_{(S)}$ leads to size distributions with a significantly broader tail for small γ , after the rescaling of the distribution. It is important to note that the lifetime of an aggregate of size larger than $\alpha_{(S)}$ is shorter than τ_f , and therefore all large aggregates, which form the tail of the size distribution, have a short free path before a breakage event occurs. Nevertheless the formation of these aggregates changes strongly the shape of the size distribution.

3. From tracers to inertial aggregates: intermediate cases.

In the previous subsections we have analyzed two limiting cases: aggregation of tracers and aggregation of inertial monomers. In these two setups we have observed that obtained aggregate size distributions in the steady state for different γ values can all be rescaled by a characteristic aggregate size, $\langle \alpha \rangle_e$ suggested from Eq.(3). This average aggregate size $\langle \alpha \rangle_e$, in turn grows algebraically with the binding strength. Here in this final subsection we study the scaling properties of the steady state size distribution for suspensions of aggregates with intermediate inertial properties and show cases where the size distribution changes its shape with changes in γ . We show simple examples where the dynamics of an average size is equivalent to tracers for small γ values and to inertial aggregate for large γ values. We speculate that the enhancement of aggregation rates for inertial monomers arises from the interplay of two effects: it is, more importantly, a result of differences in reaction times in the advection between aggregates of different sizes (as the range of sizes increases so does the range of Stokes times τ_α); and also, to a smaller degree, a result of preferential concentration, which is significant for some size classes only. Although the second phenomenon has a strong impact only for aggregates with Stokes time ~ 1 , the first one depends on the variety of sizes in the suspension. Here we analyze in detail this interplay, and to this end we introduce two additional monomer types, which exhibit intermediate properties between tracers and inertial aggregates: small inertial monomers ($St = 0.08$ and $\beta = 0.1$); and weakly inertial monomers ($St = 0.08$ and $\beta = 0.99$).

Firstly, we compare the aggregation dynamics of tracers and for inertial particles, and distinguish the four types of monomers: (i) inertial, (ii) small inertial, (iii) weakly inertial and (iv) tracers. The differences can be observed already in the transient dynamics. As we can see from Fig. 9 (a), the transients in the dynamics of small inertial and inertial monomers (cases (i) and (ii), almost indistinguishable in Fig. 9 (a)) are much shorter than of the weakly inertial and tracer cases. Inertial aggregates also grow to larger sizes, and the mean size has stronger and more frequent fluctuations, indicating the presence of a larger number of aggregation and fragmentation events. The short transients and a large average size are both consequences of an increase in collision rates due to inertial effects. The mass quickly flows towards larger sizes, and we obtain a broad size distribution, see squares in Fig. 9 (b).

The average aggregate size $\langle \alpha \rangle_e$ in the suspension is comparatively smaller for both tracer monomers (black line in Fig. 9 (a)) and weakly inertial monomers (blue line in Fig. 9 (a)). This is because, as tracers, weakly inertial monomers also have the tendency to distribute themselves nearly homogeneously in space, while advected by an incompressible flow. Although, for the chosen value of γ , inertial effects appear to be small, we can still notice

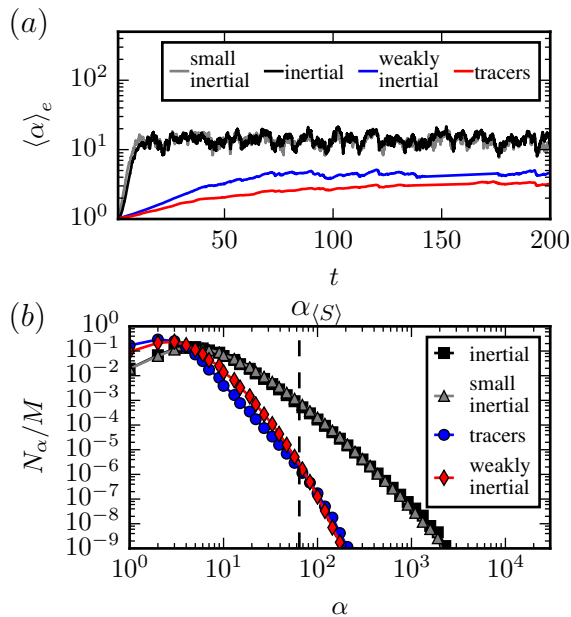


FIG. 9. (a) Time evolution of the average aggregate size in the suspension. (b) Size distribution of aggregates in the steady state. Each ensemble contained 10^6 monomers and the binding strength between monomers was $\gamma = 4$.

their influence in both the duration of transients and the average aggregate size, see Fig. 9. While tracers collide only due to spatial variations of the velocity field [9], the drag force makes trajectories of aggregates formed by weakly inertial monomers deviate from the underlying flow. As differences in sizes of these aggregates increase, so does the range of Stokes times of these aggregates. They all react differently to the velocity field, which results in an enhancement of collision rates. This influences the average size and the shape of the aggregate size distribution in the steady state, Fig. 9 and Fig. 11. It is important to emphasize that the inertial effects grow with an increase in the variety of different sizes in the ensemble. This in turn boosts the flux of mass towards large sizes generating a positive feedback.

Secondly we compare the effect of variations of binding strength for tracers and our three types of inertial aggregates. These results are summarized in Fig. 10. The average aggregate size $\langle \alpha \rangle_t$ always grows with γ , but as already demonstrated for the size distribution the steady state may show different properties for small and large values of γ . Fig. 10 shows that the mean aggregate size $\langle \alpha \rangle_t$ scales as γ^ω (with $\omega \sim 2.5$ for inertial aggregates and $\omega \sim 3$ for tracers). The scaling of the average size with γ for the suspension with tracer monomers, directly reflects the fact that the smallest aggregate in the suspension grows as $\propto \gamma^3$ and the dynamics of motion for these aggregates does not depend on their size. By contrast, for inertial monomers the properties of smallest aggregates in the suspension do change. As the “effective monomers”, the smallest unbreakable aggregates, increase in size with

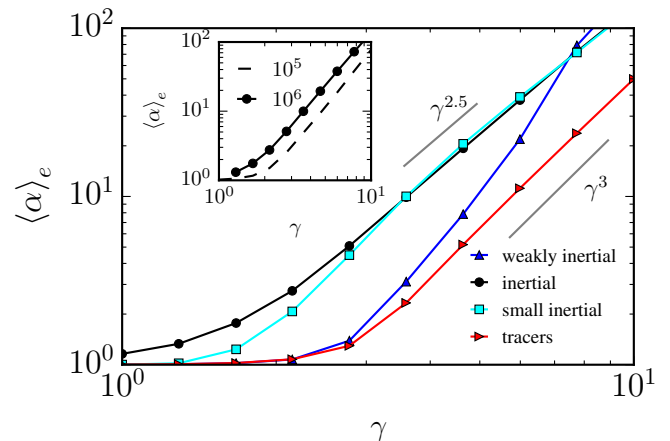


FIG. 10. Average aggregate size in the steady state $\langle \alpha \rangle_t$ for inertial ($St = 0.83$, $\beta = 0.1$), small inertial ($St = 0.08$, $\beta = 0.1$), weakly inertial ($St = 0.08$, $\beta = 0.99$) and tracer aggregates changing the binding strength γ , the simulation was initialized with $M = 10^6$. The inset shows $\langle \alpha \rangle_t$ for a system with 10^6 (black dots) and another with 10^5 (dashed line) monomers, characterized by $\beta = 0.1$.

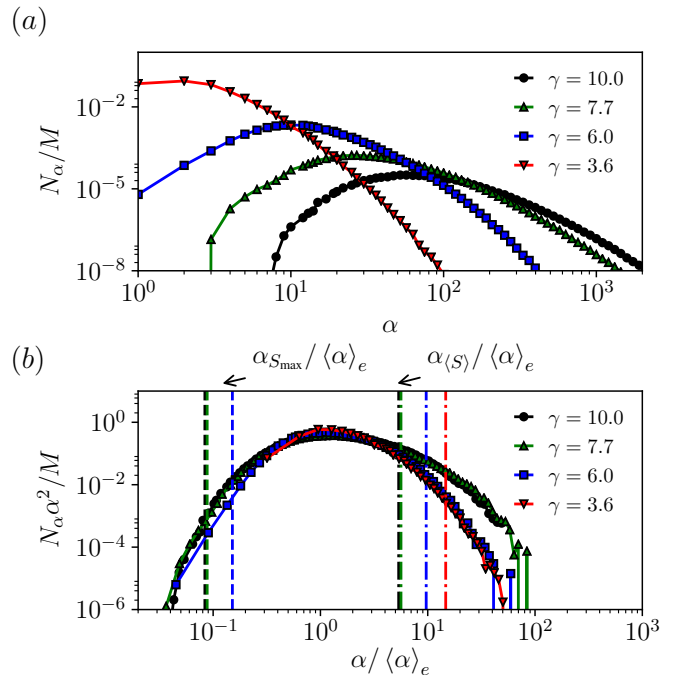


FIG. 11. Steady state size distribution for weakly inertial monomers ($St = 0.08$, $\beta = 0.99$). The simulation contains 10^6 monomers. (a) The size distribution in its original form. (b) Rescaled size distribution according to Eq.(3).

γ they start to spread homogeneously in space, and preferential concentration is decreased. However, the differences in Stokes times of aggregates formed in the suspension still have a strong effect in keeping the aggregation rates higher than that of these tracer monomers. A change in dynamics is also noticeable for small inertial

monomers (with $St = 0.08$, $\beta = 0.1$). For small γ they behave as tracers but with stronger binding forces they can form “effective monomers” that are large enough to experience the influence of the drag. At this value of binding strength the average aggregate produced in the steady state by small inertial monomers is identical to the one produced by aggregation-fragmentation dynamics of inertial monomers ($St = 0.83$, $\beta = 0.1$). For weakly inertial monomers (blue triangles Fig. 10) this transition in the dynamics is even more pronounced. Here the increase of binding strength leads to a strong modification of the shape of the steady state size distributions. As a consequence, size distributions formed by monomers possessing different values of γ cannot be rescaled into a similar form with the use of Eq.(3), see Fig. 11.

IV. CONCLUSION

We have investigated aggregation and fragmentation dynamics of tracers and inertial aggregates in random flows. We have used an individual particle based model to compute the motion of aggregates, characterizing each one of them by its coordinates in space, its velocity and its size. Furthermore, the computation of individual trajectories made it possible to exactly evaluate breakup events that depend on local hydrodynamic forces. Throughout this work we have compared properties of the steady-state for several ensembles, where we have varied the monomer’s Stokes number and density. Our objective was to analyze the influence of aggregation on the steady-state size distributions, which result from differences in the advection dynamics. While the equations of motion are independent of aggregate sizes for tracer aggregates, for inertial ones they depend on the sizes present in the suspension. We also analyzed the dependency on the number of monomers (i.e. the solid fraction) and their binding strength, both of which change the average aggregate size in the steady-state $\langle \alpha \rangle_t$, albeit in different ways.

We observe that beside the expected result that the size distribution gets broader for all ensemble types as the number of monomers increases, we also observe that the shape of these size distributions change as well. These changes are especially noticeable in the distribution tail, while the average aggregate size grows with $M^{0.15}$ for tracers and $M^{0.3}$ for inertial aggregates. In contrast to predictions by mean field theory we do not find a characteristic size able to rescale the distribution into a single shape. We interpret that these differences in the shape of the distribution follow from an interplay between the collision and flow time scales, since with an increase in M more aggregation events can occur within the correlation time of the flow. In addition to this, we have also the correlation between particle sizes and the local magnitude of the shear forces, which should also contribute to the deviation from what is expected in a mean-field

scenario.

The increase in the binding strength also results in broader size distributions. Additionally, we have observed that for each one of the two limiting cases — tracer and inertial monomers — it is possible to identify a characteristic size which allows us to rescale the size distribution into an almost universal shape (with deviations only in the tail). In case of tracers, this characteristic size is either the smallest particle in the steady state (the “effective monomer”), or the average aggregate size in the steady state, which grows as γ^3 . In the case of inertial monomers, only the average aggregate size can be used as the characteristic size for the scaling, which in turn grows as $\gamma^{2.5}$. This smaller exponent is a result of a decrease in the preferential concentration experienced by the “effective monomers”. The weaker preferential concentration for larger γ values brings the average size closer to the one characterizing a system of tracers, where the spatial distribution of aggregates is homogeneous. Finally, we have also analyzed monomers with intermediate inertial properties, i.e. small Stokes numbers and almost neutrally buoyant. In both cases the scaling failed, since with an increase in γ these systems shift from a tracer-like to an inertial-like behaviour. During this transition, the size distributions exhibits different shapes, according to the inertial properties of the aggregates present in the steady state.

Another aspect which we would like to bring to attention is that in real world systems not all collision events result in aggregation, i.e. aggregation occurs only with a certain probability corresponding to a collision efficiency. Furthermore, there should be a direct relation between binding strength γ and the value for this collision efficiency, since both represent interactions among parts of an aggregate. It was shown in [5] that the effects of collision efficiency on the size distribution is equivalent to the influence of the dilution rate. Although in this work we have decided for decoupling the two aspects, one can guess the combined results from simultaneous changes in γ and M .

In summary, we have showed how differences in the advection and subsequently in collision dynamics impact on the steady state size distribution of aggregation and fragmentation processes. We have demonstrated the applicability of the scaling relation provided by the mean-field theory of reversible aggregation for our individual based approach and also demonstrated when this relation fails. Our results show that it is important to take into account that inertial aggregates change their advection dynamics with changes in their size.

Finally, we would like to briefly mention the possibility of applying this approach to the formation and settling of marine snow. These aggregates are almost neutrally buoyant, with densities close to the water density (as in our case of weakly inertial aggregates). For this reason, these aggregates have an almost homogeneous distribution in the flow [43]. Through a sequence of aggregation and fragmentation events, these aggregates reach a given

size distribution while advected by the flow field. Because they are very light particles, the fragmentation events are triggered by the hydrodynamic stress. Although their horizontal motion and dispersion are similar to tracers, they also sediment, and as a consequence their settling speed is determined by the aggregate size, and thus is tightly linked to the aggregation and fragmentation processes. It is therefore very important to correctly determine the balance between aggregation and fragmentation to evaluate the settling velocity for marine snow. Our results suggest that even for such light particles the inertial properties of a characteristic aggregate size (average size) may influence the overall shape of the size distribution.

V. ACKNOWLEDGMENTS

We are grateful to George Jackson, Tamás Tél, Jöran März and Jens Zahn for illuminating discussions.

Appendix A

Here we describe the core aspects of the random velocity field (also known as synthetic/kinematic turbulence) which was used for our simulations. It is based on statistical properties of homogeneous, isotropic and stationary turbulence and is constructed in such a way to contain predominately one length for its coherent structures (λ_f) and be characterized by a single correlation time scale (τ_f). Therefore, although the random flow is unable to take into account the interplay of the large variety of scales present in a turbulent flow field, it mimics its main statistical properties such as correlations and the energy spectrum with a lower computational effort. More details of the implementation and properties of random flows can be found in [23, 28, 44].

For our simulations we assume a two dimensional (2D) and incompressible velocity field $\mathbf{u}(\mathbf{r}, t)$, which extends

over a periodic box with dimensions of $L \times L$. The incompressibility ($\nabla \cdot \mathbf{u} = 0$) of the flow allows us to introduce a stream function ψ defined as:

$$\mathbf{u}(\mathbf{r}, t) = \left(\frac{\partial \psi}{\partial y}, -\frac{\partial \psi}{\partial x} \right). \quad (\text{A1})$$

This stream function is assumed to have Gaussian, Markovian statistics and to be describable by an Ornstein-Uhlenbeck process. To establish proper spatial correlations it is convenient to treat the process in Fourier space

$$\psi(\mathbf{r}, t) = \frac{\sqrt{\pi}}{L} \sum_{\mathbf{k}} \psi_{\mathbf{k}}(t) e^{i\mathbf{k} \cdot \mathbf{r}}, \quad (\text{A2})$$

$$\psi_{\mathbf{k}}(t + \delta t) = \psi_{\mathbf{k}}(t) \left(1 - \frac{\delta t}{\tau_f} \right) + u_0 \lambda_f^2 Q(\lambda_f, \mathbf{k}) \sqrt{\frac{\delta t}{\tau_f}} w_{\mathbf{k}}. \quad (\text{A3})$$

Where τ_f and λ_f are respectively the correlation time and length, u_0 is the characteristic velocity and $Q(\lambda_f, \mathbf{k})$ is chosen according to the energy spectrum used. The noise is introduced through $w_{\mathbf{k}}$, which are complex Gaussian random numbers which have zero mean and are delta correlated,

$$\langle w_{\mathbf{k}} \rangle = 0, \quad w_{\mathbf{k}^*} = -w_{\mathbf{k}} \quad \text{and} \quad \langle w_{\mathbf{k}} w_{\mathbf{k}'} \rangle = \delta_{\mathbf{k}\mathbf{k}'} \quad (\text{A4})$$

for more details see [22].

The energy spectrum we consider in our simulation is the Kraichnan's spectrum:

$$E(k) \propto k^3 e^{-\lambda_f^2 k^2} = k^3 Q^2(\lambda_f, k). \quad (\text{A5})$$

However, it is important to note that the spectrum is not well resolved for $\frac{L}{\lambda_f} < 10$, and one single length scale dominates as the characteristic vortex size.

-
- [1] G. Falkovich, A. Fouxon, and M. G. Stepanov, *Nature* **419**, 151 (2002).
 - [2] A. B. Burd and G. A. Jackson, *Annual Review of Marine Science* **1**, 65 (2009), 00081.
 - [3] J. Maerz, R. Verney, K. Wirtz, and U. Feudel, *Continental Shelf Research* **31**, S84 (2011).
 - [4] J. Silk, *Star formation*, edited by Schweizerische Gesellschaft für Astrophysik und Astronomie (Geneva Observatory, Sauverny, Switzerland, 1980).
 - [5] J. C. Zahn and U. Feudel, *Nonlin. Processes Geophys.* **16**, 677 (2009).
 - [6] J. C. Zahn, J. Maerz, and U. Feudel, *Physica D: Nonlinear Phenomena* **240**, 882 (2011).
 - [7] J. C. Zahn, R. D. Vilela, U. Feudel, and T. Tél, *Physical Review E* **80**, 026311 (2009).
 - [8] J. C. Zahn, R. D. Vilela, U. Feudel, and T. Tél, *Physical Review E* **77**, 055301 (2008).
 - [9] P. G. Saffman and J. S. Turner, *Journal of Fluid Mechanics* **1**, 16 (1956).
 - [10] J. Bec, A. Celani, M. Cencini, and S. Musacchio, *Physics of Fluids (1994-present)* **17**, 073301 (2005), 00062.
 - [11] J. Eaton and J. Fessler, *International Journal of Multiphase Flow* **20**, **Supplement 1**, 169 (1994), 00472.
 - [12] L.-P. Wang and M. R. Maxey, *Journal of Fluid Mechanics* **256**, 27 (1993).
 - [13] M. Wilkinson and B. Mehlig, *EPL (Europhysics Letters)* **71**, 186 (2005).
 - [14] M. Wilkinson and B. Mehlig, *Physical Review E* **68**, 040101 (2003).
 - [15] A. Pumir and M. Wilkinson, *Annual Review of Condensed Matter Physics* **7**, 141 (2016).
 - [16] M. U. Babler, L. Biferale, and A. S. Lanotte, *Physical*

- Review E **85**, 025301 (2012), 00003.
- [17] M. U. Bäbler, L. Biferale, L. Brandt, U. Feudel, K. Guseva, A. S. Lanotte, C. Marchioli, F. Picano, G. Sardina, A. Soldati, and F. Toschi, *Journal of Fluid Mechanics* **766**, 104 (2015).
- [18] P. T. Spicer and S. E. Pratsinis, *AIChE Journal* **42**, 1612 (1996).
- [19] M. U. Bäbler and M. Morbidelli, *Journal of Colloid and Interface Science* **316**, 428 (2007).
- [20] E. Ben-Naim and P. L. Krapivsky, *Physical Review E* **77**, 061132 (2008).
- [21] H. Sigurgeirsson, A. Stuart, and W.-L. Wan, *Journal of Computational Physics* **172**, 766 (2001), 00060.
- [22] J. García-Ojalvo, J. M. Sancho, and L. Ramírez-Piscina, *Physical Review A* **46**, 4670 (1992).
- [23] A. C. Martí, J. M. Sancho, F. Sagués, and A. Careta, *Physics of Fluids* **9**, 1078 (1997), 00037.
- [24] R. Gatignol, *J. Mec. Theor. Appl* **1**, 143 (1983).
- [25] M. R. Maxey, *Physics of Fluids* **26**, 883 (1983).
- [26] T. R. Auton, J. C. R. Hunt, and M. Prud'Homme, *Journal of Fluid Mechanics* **197**, 241 (1988), 00348.
- [27] J. Bec, L. Biferale, G. Boffetta, A. Celani, M. Cencini, A. Lanotte, S. Musacchio, and F. Toschi, *Journal of Fluid Mechanics* **550**, 349 (2006), 00123.
- [28] H. Sigurgeirsson and A. M. Stuart, *Physics of Fluids* **14**, 4352 (2002).
- [29] K. Gustavsson and B. Mehlig, *EPL (Europhysics Letters)* **96**, 60012 (2011), 00008.
- [30] M. B. Pinsky and A. P. Khain, *Journal of Aerosol Science* **28**, 1177 (1997).
- [31] F. Family, P. Meakin, and J. M. Deutch, *Physical Review Letters* **57**, 727 (1986).
- [32] M. H. Ernst and P. G. J. van Dongen, *Physical Review A* **36**, 435 (1987).
- [33] P. Meakin and M. H. Ernst, *Physical Review Letters* **60**, 2503 (1988).
- [34] P. Meakin, *Physica Scripta* **46**, 295 (1992).
- [35] A. Zaccone, M. Soos, M. Lattuada, H. Wu, M. U. Bäbler, and M. Morbidelli, *Physical Review E* **79**, 061401 (2009).
- [36] J. De Bona, A. S. Lanotte, and M. Vanni, *Journal of Fluid Mechanics* **755**, 365 (2014).
- [37] It is important to note that the fragmentation by hydrodynamic forces is observed to be the most relevant fragmentation mechanism only for light particles.
- [38] In particular, for a turbulent flow, it is also useful to relate the shear, to the dissipation rate by $\epsilon = \nu S$, where ν corresponds to the kinematic viscosity of the fluid.
- [39] D. S. Parker, W. J. Kaufman, and D. Jenkins, *Journal of the Sanitary Engineering Division* **98**, 79 (1972).
- [40] P. Jarvis, B. Jefferson, J. Gregory, and S. A. Parsons, *Water Research* **39**, 3121 (2005).
- [41] M. A. Delichatsios, *Physics of Fluids (1958-1988)* **18**, 622 (1975).
- [42] B. W. Zeff, D. D. Lanterman, R. McAllister, R. Roy, E. J. Kostelich, and D. P. Lathrop, *Nature* **421**, 146 (2003).
- [43] K. Guseva, A. Daitche, U. Feudel, and T. Tél, *Physical Review Fluids* **1**, 074203 (2016).
- [44] A. Careta, F. Sagués, and J. M. Sancho, *Physical Review E* **48**, 2279 (1993), 00042.